Supplementary Information for

Metagenomics-informed soil biogeochemical models projected less carbon loss in tropical soils in response to climate warming

Yang Song[a,b], Qiuming Yao[c,d], Xiaojuan Yang[b], S. Joseph Wright[g], Gangsheng Wang[b,j],Terry C. Hazen[e,f], Benjamin L. Turner[g], Malak M. Tfaily[h,l], Ljiljana Paša-Tolic[h], Eric R. Johnston[i], Minjae Kim[i], Konstantinos T. Konstantinidis[i], Chongle Pan[c,k], and Melanie A. Mayes[b]

[a] Department of Hydrology and Atmospheric Science, the University of Arizona, Tucson, AZ 85721-0011USA

[b]Climate Change Science Institute and Environmental Sciences Division, Oak Ridge National Laboratory, Oak Ridge, TN 37830 USA

[c]Computer Science and Mathematics Division, Oak Ridge National Laboratory, Oak Ridge, TN 37830 USA

[d]Department of Computer Science and Engineering, the University of Nebraska-Lincoln, Lincoln, NE 68588-0115 USA

[e]Biosciences Division, Oak Ridge National Laboratory, Oak Ridge, TN 37830 USA

[f]Department of Civil and Environmental Engineering, University of Tennessee, Knoxville, TN 37996 USA

[g]Smithsonian Tropical Research Institute, Apartado 0843-03092, Balboa, Ancon, Republic of Panama

[h]Environmental Molecular Sciences Laboratory and Biological Sciences Division, Pacific Northwest National Laboratory, Richland, WA 99352 USA

[i]School of Civil and Environmental Engineering, Georgia Institute of Technology

[j]Institute for Environmental Genomics and Department of Microbiology and Plant Biology, University of Oklahoma, Norman, OK 73019 USA

[k]Department of Microbiology and Plant Biology, University of Oklahoma, Norman, OK 73019 USA

[l]Department of Environmental Science, the University of Arizona, Tucson, AZ 85721 USA

*Yang Song and Melanie A. Mayes

Email: chopinsong@arizona.edu and mayesma@ornl.gov

This PDF file includes:

Supplementary Methods S1-S8
Supplementary Equations S1-S92
Supplementary Figures S1 to S5
Supplementary Tables S1 to S3
Supplementary Notes

Supplementary Methods

1. Projection of soil carbon dynamics in response to climate change

To test how metagenomics-informed functional diversity and environmental acclimation of microbial communities affect soil carbon dynamics in response to projected climate change in Panama, we built upon the modeled microbial dynamics and soil condition in 2014 and further performed simulations over the period of 2015-2100 with $CoMEND_L$, $CoMEND_M$, $CoMEND_H$, and $CoMEND_{HD}$, respectively. Each model was driven by simulated daily soil moisture and soil temperature, litter input and plant P rates from the CESM large ensemble projection under the RCP8.5 scenarios. The CESM-projected climate forcing indicated that the mean annual soil temperature increased to 2.6 °C by the year 2100, while soil moisture has no significant trend over the 2015-2100 in Panama[1]. To test how this warming trend will affect the projected soil carbon dynamics by different versions of CoMEND, we performed two simulations by each model. The Simulation I was driven by the detrended soil temperature and soil moisture projected by the climate model. The Simulation II was driven by the projected soil temperature and detrended soil moisture data. Then the difference in the simulated SOM between the Simulation II and the Simulation I was defined as the effect of warming on projected soil carbon dynamics.

2. SOM analysis with Electrospray Ionization Fourier Transformed Ion Cyclotron Resonance Mass Spectrometry (ESI-FTICR MS)

We performed ESI-FTICR MS analysis to analyze the relative abundance of SOM compounds (lignin-like, carbohydrate-like, etc.) in the control and P-fertilized plots, as described previously[2,3]. Briefly, 1g bulk soil samples were sequentially extracted using three solvents with decreasing polarity (water-methanol-chloroform). The high-resolution mass spectra of the SOM in the extracts were collected in the negative ion mode on a 12 Tesla Bruker SolariX FGICR spectrometer. ESI-FTICR MS data were acquired for the mass to charge ratio (m/z) in the range of 112 to 1333 with an ion accumulation time of 0.1 s. One hundred forty-four scans were averaged for each sample and internally calibrated using OM homologous series separated by 14 Da (–CH_2 groups). Molecular formulae were assigned based on the following criteria: S/N >7, and mass measurement error <1 ppm, taking into consideration the presence of C, H, O, N, S and P and excluding other elements. Peaks with large mass ratios (m/z values >500 Da) were assigned formulae through propagation of CH_2, O, and H_2 homologous series. The fractions of different biochemical classes of compounds (lignin-like, carbohydrate-like, etc.) were calculated based on their hydrogen-to-carbon and oxygen-to-carbon atomic ratios, as described previously[4]. This ESI-FTICR MS measurement together with reported soil organic matter and inorganic N and P components at Panama site [5-7] were used to inform enzyme available SOM compounds. Integrating this information with omics-informed soil enzyme information allowed us to identify existing SOM decomposition pathways in Panamanian soils (Fig. S1-S3).

3. A summary of the equations in the CoMEND model

There are 15 microbial-activated SOM (ASOM), 15 mineral-protected SOM (MSOM), and 15 adsorbed SOM (QSOM) pools in the CoMEND model (Supplementary Equations). The decomposition of each ASOM pool is catalyzed by the corresponding enzyme functional class (EFC) described by the Michaelis-Menten equation (Eqs. S1-S3). The dynamic adsorption of each ASOM pool to the corresponding QSOM pool is simulated as a function of the pool size of ASOM and mineral surface coverage defined as the ratio of actual adsorbed ASOM content to the maximum adsorption capacity (Qmax) of each QSOM pool (Eqs. S4-S7). The desorption of each QSOM pool to the corresponding ASOM pool is only controlled by the mineral surface coverage (Eqs. S8-S11). The mutual conversion between QSOM and MSOM pools follows the same equation as that used for simulating the mutual conversion between ASOM and QSOM pools, but with a lower desorption rate and larger maximum adsorption capacity (Eqs. S12-S19).

The original MEND model lacked a P cycle process. We incorporated inorganic P conversion processes into the CoMEND model following the Community Land Model (CLM)-CNP[8,9]. There are five inorganic P (IP) pools in the CoMEND model: dissolved IP (DIP), labile IP (QIP), secondary mineral IP (SIP), parent material P (PIP), and occluded IP (OIP). The rate of PIP weathering, SIP occlusion and desorption and DIP adsorption are simulated through the first-order rate processes (Eqs. S20-S23). Instead of using the first order rate equation as in the MEND model and the CLM-CNP model, we applied the Michaelis-Menten equation to simulate the enzyme-mediated DIP immobilization, monomer biochemical P

mineralization and biological P mineralization, biological N-mineralization, and other inorganic N transformation processes (e.g., nitrification, denitrification and microbial N assimilation etc.) (Eqs. S24-S31). The microbial growth and maintenance, dormancy and mortality and enzyme synthesis and deactivation are simulated following the MEND model (Eqs. S32-S40). The dynamics of each SOM pool and inorganic N and inorganic P pool are listed in Supplementary Equations (Eqs. S41-S92).

4. Parameterization of the dynamic EFC allocation scheme for resource acquisition

A metagenomics-informed dynamic EFC allocation scheme was developed to parameterize adaptive microbial responses to environmental perturbation. This scheme assumes that the allocation of microbially-synthesized enzymes to each EFC varies with the availability of C, nutrients and soil water in order to maximize the acquisition of limiting resources and minimize energy consumption and osmotic stress. The limitation factors for C, N, P, and soil water (L_C, L_N, L_P, L_W) are calculated as follows

$$\begin{cases} L_C = max\left\{min\left[1.0, max\left(0., \frac{CN_{MB}-CN_{MB_{avg}}}{CN_{MB_{min}}-CN_{MB_{avg}}}\right)\right], min\left[1.0, max\left(0., \frac{CP_{MB}-CP_{MB_{avg}}}{CP_{MB_{min}}-CP_{MB_{avg}}}\right)\right]\right\} \\ L_N = \min\left[1.0, \max\left(0., \frac{CN_{MB}-CN_{MB_{avg}}}{CN_{MB_{max}}-CN_{MB_{avg}}}\right)\right] \\ L_P = \min\left[1.0, \max\left(0., \frac{CP_{MB}-CP_{MB_{avg}}}{CP_{MB_{max}}-CP_{MB_{avg}}}\right)\right] \\ L_W = \frac{|\psi|^b}{|\psi|^b+|\psi_D|^b} \end{cases} \quad \text{Eq. S112}$$

where CN_{MB} is the microbial C/N ratio at the current time step. $CN_{MB_{avg}}$, $CN_{MB_{min}}$ and $CN_{MB_{max}}$ are the averaged, minimum and maximum microbial C/N ratio, respectively. CP_{MB} is the microbial C/P ratio at the current time step. $CP_{MB_{avg}}$, $CP_{MB_{min}}$ and $CP_{MB_{max}}$ are the averaged, minimum, and maximum microbial C/P ratio, respectively. The water limitation factor is the same as the soil water response function for microbial mortality rate (Eq. S107). The exponent b describes the steepness of the water limitation factor curve, and ψ_D is the critical soil water potential parameter depending on the osmolyte synthesis strategy[10]. Thus, L_W reflects drying-induced matric stress and osmotic stress[11]. The values of L_C, L_N, L_P and L_W varied from 0 to 1. The closer the values are to 1, the stronger the limitation of C, N, P, and soil water.

The CoMEND model assigns microbially synthesized enzymes to 22 EFCs (f_{C_i} , f_{N_j} , f_{P_k}) and other non-defined functional enzymes (f_U) as follows.

$$f_{C_i} = \begin{cases} \frac{\sum f0_{C_i}+w_{N1}L_N+w_{P1}L_P+w_{W1}L_W}{1.0+w_CL_C+w_NL_N+w_PL_P+w_WL_W}\alpha_{C_i}, & i = endo1, exo, oligo \\ \frac{f0_{C_i}+w_{C1}L_C}{1.0+w_CL_C+w_NL_N+w_PL_P+w_WL_W}, & i = endo2 \end{cases} \quad \text{Eq. S113}$$

$$f_{N_j} = \begin{cases} \frac{\sum f0_{N_j}+w_{N2}L_N+w_{P2}L_P+w_{W2}L_W}{1.0+w_CL_C+w_NL_N+w_PL_P+w_WL_W}\alpha_{N_j}, & j = endo1, exo1, exo2 \\ \frac{\sum f0_{N_j}+w_{C2}L_C+w_{N3}L_N}{1.0+w_CL_C+w_NL_N+w_PL_P+w_WL_W}\alpha_{N_j}, & j = oligo1, oligo2, inN1, inN3 \\ \frac{f0_{N_j}+w_{P3}L_P}{1.0+w_CL_C+w_NL_N+w_PL_P+w_WL_W}, & j = mono \\ \frac{f0_{N_j}}{1.0+w_CL_C+w_NL_N+w_PL_P+w_WL_W}\alpha_{N_j}, & j = inN2, inN4 \end{cases} \quad \text{Eq. S114}$$

$$f_{P_k} = \frac{\sum f0_{P_k}+w_{P4}L_P+w_{W3}L_W}{1.0+w_CL_C+w_NL_N+w_PL_P+w_WL_W}\alpha_{P_k}, \quad \begin{matrix} k = exo1, oligo1, exo2, oligo2, \\ mono1, mono2, mono3, inP \end{matrix} \quad \text{Eq. S115}$$

$$f_U = \max\left(0.0, \left(1.0 - \sum f_{C_i} - \sum f_{N_j} - \sum f_{P_k}\right)\right) \quad \text{Eq. S116}$$

Here the values of w_C, w_N w_P and w_W represent the sensitivity of overall enzyme allocation to limitation of C, N, P, and soil water, respectively. The w_{Ci} (i = 1,2), w_{Nj} (j = 1,2,3) and w_{Pk} (k = 1,2,3,4) , w_{wl} (l = 1,2, 3)and represent the sensitivity of specific EFC allocation to the limitation of C, N, P, and soil water, where $w_C = \sum w_{Ci}$, $w_N = \sum w_{Nj}$, $w_P = \sum w_{Pk}$, and $w_w = \sum w_{wl}$. Here w_{Ci}, w_{Nj}, w_{Pk} and w_{wl} depend on metagenomics-informed tradeoffs between enzyme allocation and energy investment, and osmolyte

synthesis and can be validated by integrated effect size of each EFC in response to nutrient and water stresses.

To maximize nutrient acquisition and minimize energy consumption, the microbial community prefers to allocate more synthesized enzymes to EFCs for lignin decomposition under the C-limited condition (Eq. S113), to EFCs for N-containing SOM decomposition and inorganic N transformation under the N-limited condition (Eq. S114) and to EFCs for P-containing SOM decomposition under the P-limited condition (Eq. S115). Also, the microbial community allocates enzymes to EFCs for decomposing complex carbohydrates and N-containing SOM (e.g., large polymers of proteins) under P-limited conditions (Eqs. S113-114) and to EFCs for decomposing complex carbohydrates under N-limited condition (Eq. S114). When a resource can be acquired from multiple substrates, the total enzyme allocation for acquiring this resource is weighted by the corresponding EFC allocation weighting factors (α_{C_i}, α_{N_j}, α_{P_k}) to calculate the EFC-specific allocation factor. The α_{C_i}, α_{N_j} and α_{P_k} are expressed as the form of $\frac{\frac{Vd_{EFC}}{(Km_{EFC}/S_{EFC}+1)}}{\sum\frac{Vd_{EFC}}{(Km_{EFC}/S_{EFC}+1)}}$, where Vd_{EFC} and Km_{EFC} are the maximum specific decomposition rate and half-saturation constant for the EFC, E_{EFC}, while S_{E_m} is the pool size of SOM that the E_m catalyzes. The m denotes lignocellulose-containing SOM i, N-containing SOM j, and P-containing SOM k, respectively. The larger the values of Vd_{E_m} and S_{E_m}, the more sensitive E_m is to resource limitation.

Our metagenomics analyses at the Panama site did not have sufficient information for an examination of the response of enzyme allocation to soil water limitation. However, a metagenomic analysis in similar tropical forest soils in Puerto Rico found that microbial communities increased extracellular enzyme production for macromolecular SOM decomposition to satisfy increased C demand under water-limited conditions[12,13]. This tradeoff between enzyme allocation and water deficiency is represented by the L_W parameter-related part in Eqs. 1-3. The closer the L_W is to 1 (stronger water limitation), the more the enzyme allocation is to EFCs for macromolecular SOM decomposition.

This tradeoff between dynamic EFC allocation and water stress will in turn mitigate the microbial dormancy and mortality. This feedback is parameterized by adjusting critical soil water potential parameters (ψ_{A2D} and ψ_D) in Eqs. S109 and S107. The values of ψ_{A2D} and ψ_D indicate the soil water potential at which the dormancy or mortality rate is half the maximum dormancy or mortality rate, respectively. Therefore, the more EFCs for macromolecular SOM decomposition, the smaller the L_c value is, the larger the absolute value of ψ_{A2D} and ψ_D, and the smaller the microbial dormancy and mortality rate (Eq. S109 and Eq. S107 in Table S2).

5. Kinetic parameters in the CoMEND model

We collected the reported kinetics parameters and corresponding experimental conditions (e.g., origin, substrate, product, temperature, and pH, enzyme strain etc.) for each enzyme classification (EC) number in each EFC from the BRENDA biochemical database[14]. The final dataset contained around 4900 observations for 118 EC numbers in all EFCs. The parameters in the response functions of temperature and pH (Eqs. S100-S101) are activation energy (*Ea*), the optimal pH (pH_{opt}), and the sensitivity of the reaction rate to deviation from pH_{opt} (pH_{sen}). They were estimated with curve fitting of temperature and pH response data, if reported. We estimated the maximum specific reaction rate (*Vd*) and half-saturation constant (*Ks*) for each EC number at 20°C and optimum pH using Eq. S97. We considered difference in kinetics of each EC numbers among diverse isoenzymes by collecting data from diverse microbial source (e.g. enzymes from bacteria, fungi or archaea), habitats (soils, water, or lab), and the type of enzyme (wildtype or mutant). Here we only used kinetic parameters estimated for wildtype enzymes from bacteria with metagenomics-based taxonomic distribution analyses, which indicated high abundances of bacteria in our research soils[2]. We estimated the mean and standard deviation values of a kinetic parameter of each EC number based on these collected data. Finally, we calculated the weighted mean and the weighted standard deviation of a kinetic parameter of all EC numbers within each EFC to present the EFC-specific kinetic parameter and its variability (SI Data S4). The weighted factor was the relative gene abundance of each EC number within an EFC (SI Data S2). As enzyme composition is different within each EFC defined in $CoMEND_{HD}$, $CoMEND_H$, $CoMEND_M$, and $CoMEND_L$ (SI Data S2), estimated kinetic parameters of the EFC varies with represented functional diversity of microbial communities (SI Table S4).

6. Site-specific parameter optimization in the CoMEND model

We optimized the site-specific model parameters through the SCE (Shuffled Complex Evolution) algorithm[15,16]. This parameter optimization aims to minimize the total objective function (J), estimated as the weighted average of multiple single-objectives.

$$J = \sum_{i=1}^{m} w_i \times J_i, \quad \text{Eq. S117}$$

$$\sum_{i=1}^{m} w_i = 1.0, \text{ with } w_i \in (0,1), \quad \text{Eq. S118}$$

Here w_i is the weighting factor for J_i and m is the number of objective functions. Each single objective J_i is defined as (1-R^2), where R^2 is the Coefficient of Determination between the observed and modeled data. The higher the R^2 value is, the better the model performance is. To avoid over-fitting and make sure the tested differences among $CoMEND_L$, $CoMEND_M$, $CoMEND_H$ and $CoMEND_{HD}$ result from model structure differences rather than model parameters optimization, we only calibrated these site-specific parameters for $CoMEND_{HD}$ and applied them in the other version of CoMEND.

We optimized the $CoMEND_{HD}$ parameters in two steps. In the first step, we assumed that the synthesized enzymes allocated to the 22 EFCs had no change in response to resource availability. We calibrated the parameters related to microbial growth, dormancy and mortality, inorganic P conversion and SOM adsorption/desorption (SI Data S5) with five single objectives (m=5): J_1 for microbial biomass carbon, J_2 for microbial C/P ratio, J_3 for incubation CO_2 fluxes, J_4 for soil organic carbon, J_5 for the SOM C/P ratios. In the second step, the values obtained in the first step were used to calibrate the parameters for the optimal enzyme allocation strategy (SI Data S5) with five single-objectives as above (J_1,J_2,J_3,J_4,J_5) and an extra single objective J_6 for enzyme allocation to EFC in response to P-fertilization. Here the data for optimizing dynamic enzyme allocation parameters were the combined effect size for all gene-coding enzymes in each EFC. The combined effect size of each EFC was estimated based on metagenomics-informed gene abundance data. The data for optimizing other parameters were microbial biomass carbon, microbial C/P ratio, soil carbon stock, and the SOM C/P ratios over the year 2006-2007 and five days of incubated CO_2 emissions from 2014 year of soil samples in the P-fertilized plots[17].

7. Initialization of soil pools in the CoMEND model

Soil measurements were not available at the beginning of the fertilization experiment in the year 1998. We used soil data collected from the control plot on November, 2006[17] to approximate the soil physical and chemical properties before the fertilization experiments in both the control plots and the P-fertilization plots. Collected soil data included soil texture, soil pH, soil total C, N and P content, microbial C, C/N and C/P ratio, DOC content, DOM C/N and C/P ratio, and inorganic N and P content (SI Data S7).

The partitioning of total C and N between all ASOMs and MSOMs was based on reported ratio of particulate organic C (or N) to mineral organic C (or N) at the Panama site[7]. The partitioning of total P between total ASOM, total MSOM, QMOM, and five inorganic P pools was based on the Hedley fractionation analysis at the Panama site[6,18]. The N and P content of each ASOM were estimated based on the reported soil chemical composition of organic N (e.g. protein, N components in cell walls, etc.) and organic P (e.g. phytate, nucleic acids, monomer P, etc.) with a chemolytic and hydrolysis approaches[5,19]. We assumed that inositol P existed in the residue form ($AROM_7$), whereas nucleic acids, phospholipids and 60% of organic N existed in the oligopolymer form ($AOOM_5$ and $AOOM_6$) due to their rapid hydrolysis. The C content of each N-containing and P-containing ASOM was calculated by multiplying N and P content of ASOM with its C/N and C/P ratio (SI Table S3). The C content of each lignocellulose-containing ASOM (carbohydrate-related pool and lignin-related pool) was estimated based on reported lignin ratio of lignocellulose[20]. The fraction of each ASOM to total ASOMs was finally defined as the C content of the corresponding ASOM to total C in all ASOMs. We assumed the chemical composition of organic N and P in the mineral-protected SOM was similar to that in the microbial-activated SOM and then estimated the fraction of each MSOM to total MSOM following the method described above.

8. Input data for the CoMEND model

Hourly soil temperature at 10 cm depth over the 2000-2011 growing season and hourly air temperature at 1m height over the year 1998-2014 were measured at the nearby Lutz monitoring station (9.17ºN, 79.73ºW). This site is similar to our study site in forest covers and soil textures. We used the soil and air temperature measurements from the overlapping period to develop a regression relationship. This relationship was then used to generate a continuous time series of soil temperature from the observed air temperature for input to CoMEND. Hourly soil moisture was estimated by linearly interpolating weekly

soil moisture data at 10cm soil depth, which were collected at the study site for the 2006-2007 growing season[17] and the Lutz Watershed monitoring station for the rest of simulation period[21]. Monthly leaf litter, woody litter, product litter, and dust litter as well as litter nutrients ratios over the year 1998-2014 for the P-fertilized plots and control plots were collected from litter trap experiments[22,23]. The litter chemical components, e.g., fraction of lignin, carbohydrates, protein, nucleic acids, phospholipids and phytate, were attained from a previous study[24]. Monthly plant P uptake was calculated by interpolating yearly plant P uptake based on monthly net primary productivity (NPP). Here yearly plant P uptake was estimated by producing a P uptake rate on a dry weight basis for two forest species at the Panama site[25] with annual NPP, which was calculated as the sum of wood and leaves litter production[23].

Supplementary Equations: Components fluxes and dynamics of SOM pools in the CoMEND model.

1. Decomposition of $AROM_i$ (D_{AROC_i})

$$D_{AROC_i} = \frac{\boldsymbol{Vd_{E_{AROM_i}}} \times C_{E_{AROM_i}} \times AROC_i}{\boldsymbol{Ks_{E_{AROM_i}}} + AROC_i} \quad \text{Eq. S1}$$

E_{AROM_i} denotes C_{endo1}, C_{endo2}, N_{endo1}, N_{endo2}, P_{exo1}, P_{exo2} and P_{mono1} for i=1,2,3,4,5,6,7, respectively, $AROC_i$ and $C_{E_{AROM_i}}$ are C mass of $AROM_i$ and E_{AROM_i}, respectively

2. Decomposition of $ALOM_i$ (D_{ALOC_i})

$$D_{ALOC_i} = \frac{\boldsymbol{Vd_{E_{ALOM_i}}} \times C_{E_{ALOM_i}} \times ALOC_i}{\boldsymbol{Ks_{E_{ALOM_i}}} + ALOC_i} \quad \text{Eq. S2}$$

E_{ALOM_i} denotes C_{exo} and N_{exo1} for i=1,3 respectively, $ALOC_i$ and $C_{E_{AROM_i}}$ are C mass of $ALOM_i$ and E_{ALOM_i}, respectively

3. Decomposition of $AOOM_i$ (D_{AOOC_i})

$$D_{AOOC_i} = \frac{\boldsymbol{Vd_{E_{AOOM_i}}} \times C_{E_{AOOM_i}} \times AOOC_i}{\boldsymbol{Ks_{E_{AOOM_i}}} + AOOC_i} \quad \text{Eq. S3}$$

E_{AOOM_i} denotes C_{oligo}, N_{oligo1}, N_{oligo2}, P_{oligo1}, P_{oligo2} for i=2,3,4,5,6 respectively, $AOOC_i$ and $C_{E_{AOOM_i}}$ are C mass of $AOOM_i$ and E_{AOOM_i}, respectively

4. Adsorption of $AROM_i$ to $QROM_i$ (Ad_{AROC_i})

$$Ad_{AROC_i} = \boldsymbol{k_{ads_{AROM_i}}} \times \left(1 - \frac{QROC_i}{\boldsymbol{Qmax_{QROM_i}}}\right) \times AROC_i \quad \text{Eq. S4}$$

$QROC_i$ is C mass of $QROM_i$

5. Adsorption of $ALOM_i$ to $QLOM_i$ (Ad_{ALOC_i})

$$Ad_{ALOC_i} = \boldsymbol{k_{ads_{ALOM_i}}} \times \left(1 - \frac{QLOC_i}{\boldsymbol{Qmax_{QLOM_i}}}\right) \times ALOC_i \quad \text{Eq. S5}$$

$QLOC_i$ is C mass of $QLOM_i$

6. Adsorption of $AOOM_i$ to $QOOM_i$ (Ad_{AOOC_i})

$$Ad_{AOOC_i} = \boldsymbol{k_{ads_{AOOM_i}}} \times (1 - \frac{QOOC_i}{\boldsymbol{Qmax_{QOOM_i}}}) \times AOOC_i \quad \text{Eq. S6}$$

$QOOC_i$ is C mass of $QOOM_i$

7. Adsorption of DOM to $QMOM$ (Ad_{DOC})

$$Ad_{DOC} = \boldsymbol{k_{ads_{QMOM}}} \times (1 - \frac{QMOC}{\boldsymbol{Qmax_{QMOM}}}) \times \text{DOC} \quad \text{Eq. S7}$$

$QMOC$ and DOC are C mass of QMOM and DOM, respectively

8. Desorption from $QROM_i$ to $AROM_i$ (De_{QROC_i})

$$De_{QROC_i} = \boldsymbol{k_{des_{QROM_i}}} \times \frac{QROC_i}{\boldsymbol{Qmax_{QROM_i}}} \quad \text{Eq. S8}$$

9. Desorption of $QLOM_i$ to $ALOM_i$ (De_{QLOC_i})

$$De_{QLOC_i} = \boldsymbol{k_{des_{QLOM_i}}} \times \frac{QLOC_i}{\boldsymbol{Qmax_{QLOM_i}}} \quad \text{Eq. S9}$$

10. Desorption of $QOOM_i$ to $AOOM_i$ (De_{QOOC_i})

$$De_{QOOC_i} = \boldsymbol{k_{des_{QOOM_i}}} \times \frac{QOOC_i}{\boldsymbol{Qmax_{QOOM_i}}} \quad \text{Eq. S10}$$

11. Desorption of $QMOM$ to DOM (De_{QMOC})

$$De_{QMOC} = \boldsymbol{k_{des_{QMOM}}} \times \frac{QMOC}{\boldsymbol{Qmax_{QMOM}}} \quad \text{Eq. S11}$$

12. Conversion from $QROM_i$ to $MROM_i$ (Ad_{QROC_i})

$$Ad_{QROC_i} = \boldsymbol{k_{ads_{QROM_i}}} \times \left(1 - \frac{MROC_i}{\boldsymbol{Qmax_{MROM_i}}}\right) \times QROC_i \quad \text{Eq. S12}$$

$MROC_i$ is C mass of $MROM_i$

13. Conversion from $MROM_i$ to $QROM_i$ (De_{MROC_i})

$$De_{MROC_i} = \boldsymbol{k_{des_{MROM_i}}} \times \frac{MROC_i}{\boldsymbol{Qmax_{MROM_i}}} \quad \text{Eq. S13}$$

14. Conversion from $QLOM_i$ to $MLOM_i$ (Ad_{QLOC_i})

$$Ad_{QLOC_i} = \boldsymbol{k_{ads_{QLOM_i}}} \times \left(1 - \frac{MLOC_i}{\boldsymbol{Qmax_{MLOM_i}}}\right) \times QLOC_i \quad \text{Eq. S14}$$

$MLOC_i$ *is C mass of* $MLOM_i$

15. Conversion from $MLOM_i$ to $QLOM_i$ (De_{MLOC_i})

$$De_{MLOC_i} = \boldsymbol{k_{des_{MLOM_i}}} \times \frac{MLOC_i}{\boldsymbol{Qmax_{MLOM_i}}} \quad \text{Eq. S15}$$

16. The conversion from $QOOM_i$ to $MOOM_i$ (Ad_{QOOC_i})

$$Ad_{QOOC_i} = \boldsymbol{k_{ads_{QOOM_i}}} \times \left(1 - \frac{MOOC_i}{\boldsymbol{Qmax_{MOOM_i}}}\right) \times QOOC_i \quad \text{Eq. S16}$$

$MOOC_i$ is C mass of $MOOM_i$

17. The conversion from $MOOM_i$ to $QOOM_i$ (De_{MOOC_i})

$$De_{MOOC_i} = \boldsymbol{k_{des_{MOOM_i}}} \times \frac{MOOC_i}{\boldsymbol{Qmax_{MOOM_i}}} \quad \text{Eq. S17}$$

18. The conversion from $QMOM$ to $MMOM$ (Ad_{QMOC})

$$Ad_{QMOC} = \boldsymbol{k_{ads_{QMOM}}} \times \left(1 - \frac{MMOC}{\boldsymbol{Qmax_{MMOM}}}\right) \times QMOC \quad \text{Eq. S18}$$

$MMOC$ is C mass of $MMOM$

19. The conversion from $MMOM$ to $QMOM$ (De_{MMOC})

$$De_{MMOC} = \boldsymbol{k_{des_{MMOM}}} \times \frac{MMOM}{\boldsymbol{Qmax_{MMOM}}} \quad \text{Eq. S19}$$

20. PIP weathering (P_{wea})

$$P_{wea} = PIP \times \boldsymbol{\gamma_{wea}} \quad \text{Eq. S20}$$

21. SIP occlusion (P_{ocl})

$$P_{ocl} = SIP \times \boldsymbol{\gamma_{ocl}} \quad \text{Eq. S21}$$

22. SIP desorption (P_{sec})

$$P_{sec} = SIP \times \boldsymbol{\gamma_{des}} \quad \text{Eq. S22}$$

23. Adsorption of QIP ($P_{QIP_{ads}}$)

$$P_{QIP_{ads}} = QIP \times \boldsymbol{\gamma_{QIP_{ads}}} \quad \text{Eq. S23}$$

24. DIP immobilization (P_{im})

$$P_{im} = \frac{\boldsymbol{Vd_{P_{inP}}} \times P_{inP} \times DIP}{\boldsymbol{Ks_{P_{inP}}} + DIP} \quad \text{Eq. S24}$$

25. Extracellular dissolved organic P (DOP) mineralization (DOP_{mn})

$$DOP_{mn} = \frac{\boldsymbol{Vd_{P_{mono2}}} \times \mathrm{P_{mono2}} \times DOP}{\boldsymbol{Ks_{P_{mono2}}} + DOP} \quad \text{Eq. S25}$$

26. Active microbial P (P_{MBA}) mineralization (P_{mn})

$$P_{mn} = \frac{\boldsymbol{Vd_{P_{mono3}}} \times \mathrm{P_{mono3}} \times P_{MBA}}{\boldsymbol{Ks_{P_{mono3}}} + P_{MBA}} \quad \text{Eq. S26}$$

27. Active microbial N (N_{MBA}) mineralization (N_{mn})

$$N_{mn} = \frac{\boldsymbol{Vd_{N_{mono}}} \times \mathrm{N_{mono}} \times N_{MBA}}{\boldsymbol{Ks_{P_{mono}}} + N_{MBA}} \quad \text{Eq. S27}$$

28. Nitrification (N_{nitri})

$$N_{nitri} = \frac{\boldsymbol{Vd_{N_{inN1}}} \times \mathrm{N_{inN1}} \times IN_1}{\boldsymbol{Ks_{N_{inN1}}} + IN_1} \quad \text{Eq. S28}$$

29. Denitrification ($N_{denitri}$)

$$N_{denitri} = \frac{\boldsymbol{Vd_{N_{inN2}}} \times \mathrm{N_{inN2}} \times IN_2}{\boldsymbol{Ks_{N_{inN2}}} + IN_2} \quad \text{Eq. S29}$$

30. N assimilation (N_{assim})

$$N_{assim} = \frac{\boldsymbol{Vd_{N_{inN3}}} \times \mathrm{N_{inN3}} \times IN_1}{\boldsymbol{Ks_{N_{inN3}}} + IN_1} \quad \text{Eq. S30}$$

31. N fixation (N_{fix})

$$N_{fix} = \boldsymbol{Vd_{N_{inN4}}} \times \mathrm{N_{inN4}} \quad \text{Eq. S31}$$

32. DOM uptake by microbes (A_{DOC})

$$A_{DOC} = \frac{1}{\boldsymbol{Y_g}}\left(\boldsymbol{V_g} + \boldsymbol{V_m}\right)\frac{DOC \times C_{MBA}}{\boldsymbol{Ks_{DOC}} + DOC}, \; C_{MBA} \text{ is active microbial C mass} \quad \text{Eq. S32}$$

33. MBA growth respiration (Rg_a)

$$Rg_a = \left(\frac{1}{\boldsymbol{Y_g}} - 1\right)\frac{\boldsymbol{V_g} \times DOC \times C_{MBA}}{\boldsymbol{Ks_{DOC}} + DOC} \quad \text{Eq. S33}$$

34. MBA maintenance respiration (Rm_a)

$$Rm_a = (\frac{1}{\boldsymbol{Y_g}} - 1)\ \frac{\boldsymbol{V_m} \times DOC \times C_{MBA}}{\boldsymbol{Ks_{DOC}} + DOC} \quad \text{Eq. S34}$$

35. MBD maintenance respiration (Rm_d)

$$Rm_d = \boldsymbol{\beta} \times \boldsymbol{V_m} \times C_{MBD} \quad \text{Eq. S35}$$

C_{MBD} is dormant microbial C mass

36. MBA mortality ($D_{C_{MBA}}$)

$$D_{C_{MBA}} = \boldsymbol{\gamma_M} \times \boldsymbol{V_m} \times C_{MBA} \quad \text{Eq. S36}$$

37. Dormancy of MBA (C_{A2D})

$$C_{A2D} = (1 - \frac{DOC}{\boldsymbol{Ks_{DOC}} + DOC}) \times \boldsymbol{Vm_{A2D}} \times C_{MBA} \quad \text{Eq. S37}$$

38. Reactivation of MBD (C_{D2A})

$$C_{D2A} = \frac{DOC}{\boldsymbol{Ks_{DOC}} + DOC} \times \boldsymbol{Vm_{D2A}} \times C_{MBD} \quad \text{Eq. S38}$$

39. Synthesis of EFC (S_{C_E})

$$S_{C_E} = (1.0 - \gamma_M) \times V_m \times C_{MBA} \quad \text{Eq. S39}$$

40. Turnover of EFC (D_{C_E})

$D_{C_E} = \boldsymbol{\gamma_E} \times C_E$, γ_E is turnover rate of enzyme, $\gamma_E = \frac{\gamma_M \times C_{MBA}}{C_E}$ Eq. S40

C_E is C mass of all EFCs

41. The dynamics of C ($\frac{d_{\mathrm{AROCi}}}{dt}$), N ($\frac{d_{\mathrm{ARONi}}}{dt}$), and P ($\frac{d_{\mathrm{AROPi}}}{dt}$) in $AROM_i$

$$\frac{d_{\mathrm{AROCi}}}{dt} = I_i + (1 - \boldsymbol{f_{DOM}}) \times D_{C_{MBA}} \times \boldsymbol{f_{MBA_i}} - D_{AROC_i} - Ad_{AROC_i} + De_{QROC_i} \quad \text{Eq. S41}$$

$$\frac{d_{\mathrm{ARONi}}}{dt} = \frac{I_i}{CN_{I_i}} + (1 - \boldsymbol{f_{DOM}}) \times \frac{D_{C_{MBA}}}{CN_{MBA}} \times \boldsymbol{f_{MBA_i}} - \frac{D_{AROC_i}}{CN_{AROM_i}} - \frac{Ad_{AROC_i}}{CN_{AROM_i}} + \frac{De_{QROC_i}}{CN_{QROM_i}} \quad \text{Eq. S42}$$

$$\frac{d_{\mathrm{AROPi}}}{dt} = \frac{I_i}{CP_{I_i}} + (1 - \boldsymbol{f_{DOM}}) \times \frac{D_{C_{MBA}}}{CP_{MBA}} \times \boldsymbol{f_{MBA_i}} - \frac{D_{AROC_i}}{CP_{AROM_i}} - \frac{Ad_{AROC_i}}{CP_{AROM_i}} + \frac{De_{QROC_i}}{CP_{QROM_i}} \quad \text{Eq. S43}$$

I_i is litter C input into each $AROC_i$

42. The dynamics of C ($\frac{d_{\mathrm{ALOCi}}}{dt}$), N ($\frac{d_{\mathrm{ALONi}}}{dt}$), and P ($\frac{d_{\mathrm{ALOPi}}}{dt}$) in $ALOM_i$

$$\frac{d_{\mathrm{ALOCi}}}{dt} = \begin{cases} D_{AROC_i} - D_{ALOC_i} - Ad_{ALOC_i} + De_{QLOC_i} & i = 1,3 \\ 0 & i \neq 1,3 \end{cases} \quad \text{Eq. S44}$$

$$\frac{d_{\mathrm{ALONi}}}{dt} = \begin{cases} \frac{D_{AROC_i}}{CN_{AROM_i}} - \frac{D_{ALOC_i}}{CN_{ALOM_i}} - \frac{Ad_{ALOC_i}}{CN_{ALOM_i}} + \frac{De_{QLOC_i}}{CN_{QLOM_i}} & i = 3 \\ 0 & i \neq 3 \end{cases} \quad \text{Eq. S45}$$

$$\frac{d_{\mathrm{ALOPi}}}{dt} = 0 \quad \text{Eq. S46}$$

43. The dynamics of C ($\frac{d_{\mathrm{AOOCi}}}{dt}$), N ($\frac{d_{\mathrm{AOONi}}}{dt}$), and P ($\frac{d_{\mathrm{AOOPi}}}{dt}$) in $AOOM_i$

$$\frac{d_{\mathrm{AOOCi}}}{dt} = \begin{cases} D_{ALOC_i} - D_{AOOC_i} - Ad_{AOOC_i} + De_{QOOC_i}, & i = 1,3 \\ D_{AROC_i} - D_{AOOC_i} - Ad_{AOOC_i} + De_{QOOC_i}, & i = 4,5,6 \\ 0 & i = 2,7 \end{cases} \quad \text{Eq. S47}$$

$$\frac{d_{\mathrm{AOONi}}}{dt} = \begin{cases} \frac{D_{ALOC_i}}{CN_{ALOM_i}} - \frac{D_{AOOC_i}}{CN_{AOOM_i}} - \frac{Ad_{AOOC_i}}{CN_{AOOM_i}} + \frac{De_{QOOC_i}}{CN_{QOOM_i}}, & i = 1,3 \\ \frac{D_{AROC_i}}{CN_{AROM_i}} - \frac{D_{AOOC_i}}{CN_{AOOM_i}} - \frac{Ad_{AOOC_i}}{CN_{AOOM_i}} + \frac{De_{QOOC_i}}{CN_{QOOM_i}}, & i = 4,5,6 \\ 0 & i = 2,7 \end{cases} \quad \text{Eq. S48}$$

$$\frac{d_{\mathrm{AOOPi}}}{dt} = \begin{cases} \frac{D_{ALOC_i}}{CP_{ALOM_i}} - \frac{D_{AOOC_i}}{CP_{AOOM_i}} - \frac{Ad_{AOOC_i}}{CP_{AOOM_i}} + \frac{De_{QOOC_i}}{CP_{QOOM_i}}, & i = 1,3 \\ \frac{D_{AROC_i}}{CP_{AROM_i}} - \frac{D_{AOOC_i}}{CP_{AOOM_i}} - \frac{Ad_{AOOC_i}}{CP_{AOOM_i}} + \frac{De_{QOOC_i}}{CP_{QOOM_i}}, & i = 4,5,6 \\ 0 & i = 2,7 \end{cases} \quad \text{Eq. S49}$$

44. The dynamics of C ($\frac{\mathrm{dDOC}}{dt}$), N ($\frac{\mathrm{dDON}}{dt}$), and P ($\frac{\mathrm{dDOP}}{dt}$) in DOM

$$\frac{\mathrm{dDOC}}{dt} = I_{DOC} + \boldsymbol{f_{DOM}} \times D_{C_{MBA}} + D_{AROC_2} + \sum D_{AOOC_i} + A_{DOC} + D_{C_E} - Ad_{DOC} + De_{DOC} \quad \text{Eq. S50}$$

$$\frac{\mathrm{dDON}}{dt} = \frac{I_{DOC}}{CN_{I_{DOC}}} + \boldsymbol{f_{DOM}} \times \frac{D_{C_{MBA}}}{CN_{MBA}} + \sum \frac{D_{AOOC_i}}{CN_{AOOM_i}} + \frac{A_{DOC}}{CN_{DOM}} + \frac{D_{C_E}}{CN_E} - \frac{Ad_{DOC}}{CN_{DOM}} + \frac{De_{QMOC}}{CN_{QMOM}} \quad \text{Eq. S51}$$

$$\frac{\mathrm{dDOP}}{dt} = \frac{I_{DOC}}{CP_{I_{DOC}}} + \boldsymbol{f_{DOM}} \times \frac{D_{C_{MBA}}}{CP_{MBA}} + \sum \frac{D_{AOOC_i}}{CP_{AOOM_i}} + \frac{A_{DOC}}{CP_{DOM}} + \frac{D_{C_E}}{CP_E} - \frac{Ad_{DOC}}{CP_{DOM}} + \frac{De_{QMOC}}{CP_{QMOM}} - DOP_{mn} \quad \text{Eq. S52}$$

I_{DOC} is litter C input into DOM

45. The dynamics of C ($\frac{d_{\mathrm{QROCi}}}{dt}$), N ($\frac{d_{\mathrm{QRONi}}}{dt}$), and P ($\frac{d_{\mathrm{QROPi}}}{dt}$) in *QROM*$_i$

$$\frac{d_{\mathrm{QROCi}}}{dt} = Ad_{AROC_i} - De_{QROC_i} - Ad_{QROC_i} \quad \text{Eq. S53}$$

$$\frac{d_{\mathrm{QRONi}}}{dt} = \frac{Ad_{AROC_i}}{CN_{AROM_i}} - \frac{De_{QROC_i}}{CN_{QROM_i}} - \frac{Ad_{QROC_i}}{CN_{QROM_i}} \quad \text{Eq. S54}$$

$$\frac{d_{\mathrm{QROPi}}}{dt} = \frac{Ad_{AROC_i}}{CP_{AROM_i}} - \frac{De_{QROC_i}}{CP_{QROM_i}} - \frac{Ad_{QROC_i}}{CP_{QROM_i}} \quad \text{Eq. S55}$$

46. The dynamics of C ($\frac{d_{\mathrm{QLOCi}}}{dt}$), N ($\frac{d_{\mathrm{QLONi}}}{dt}$), and P ($\frac{d_{\mathrm{QLOPi}}}{dt}$) in *QLOM*$_i$

$$\frac{d_{\mathrm{QLOCi}}}{dt} = Ad_{ALOC_i} - De_{QLOC_i} - Ad_{QLOC_i} \quad \text{Eq. S56}$$

$$\frac{d_{\mathrm{QLONi}}}{dt} = \frac{Ad_{ALOC_i}}{CN_{ALOM_i}} - \frac{De_{QLOC_i}}{CN_{QLOM_i}} - \frac{Ad_{QLOC_i}}{CN_{QLOM_i}} \quad \text{Eq. S57}$$

$$\frac{d_{\mathrm{QLOPi}}}{dt} = \frac{Ad_{ALOC_i}}{CP_{ALOM_i}} - \frac{De_{QLOC_i}}{CP_{QLOM_i}} - \frac{Ad_{QLOC_i}}{CP_{QLOM_i}} \quad \text{Eq. S58}$$

47. The dynamics of C ($\frac{d_{\mathrm{QOOCi}}}{dt}$), N ($\frac{d_{\mathrm{QOONi}}}{dt}$), and P ($\frac{d_{\mathrm{QOOPi}}}{dt}$) in *QOOM*$_i$

$$\frac{d_{\mathrm{QOOCi}}}{dt} = Ad_{AOOC_i} - De_{QOOC_i} - Ad_{QOOC_i} \quad \text{Eq. S59}$$

$$\frac{d_{\mathrm{QOONi}}}{dt} = \frac{Ad_{AOOC_i}}{CN_{AOOM_i}} - \frac{De_{QOOC_i}}{CN_{QOOM_i}} - \frac{Ad_{QOOC_i}}{CN_{QOOM_i}} \quad \text{Eq. S60}$$

$$\frac{d_{\mathrm{QOOPi}}}{dt} = \frac{Ad_{AOOC_i}}{CP_{AOOM_i}} - \frac{De_{QOOC_i}}{CP_{QOOM_i}} - \frac{Ad_{QOOC_i}}{CP_{QOOM_i}} \quad \text{Eq. S61}$$

48. The dynamics of C ($\frac{d_{\mathrm{QMOC}}}{dt}$), N ($\frac{d_{\mathrm{QMOC}}}{dt}$), and P ($\frac{d_{\mathrm{QMOC}}}{dt}$) in *QMOM*

$$\frac{d_{\mathrm{QMOC}}}{dt} = Ad_{DOC} - De_{QMOC} - Ad_{QMOC} \quad \text{Eq. S62}$$

$$\frac{d_{\mathrm{QMOC}}}{dt} = \frac{Ad_{DOC}}{CN_{DOM}} - \frac{De_{QMOC}}{CN_{QMOM}} - \frac{Ad_{QMOC}}{CN_{QMOM}} \quad \text{Eq. S63}$$

$$\frac{d_{\mathrm{QMOC}}}{dt} = \frac{Ad_{DOC}}{CP_{DOM}} - \frac{De_{QMOC}}{CP_{QMOM}} - \frac{Ad_{QMOC}}{CP_{QMOM}} \quad \text{Eq. S64}$$

49. The dynamics of C ($\frac{d_{\mathrm{MROCi}}}{dt}$), N ($\frac{d_{\mathrm{MRONi}}}{dt}$), and P ($\frac{d_{\mathrm{MROPi}}}{dt}$) in *MROM*$_i$

$$\frac{d_{\mathrm{MROCi}}}{dt} = Ad_{QROC_i} - De_{MROC_i} \quad \text{Eq. S65}$$

$$\frac{d_{\mathrm{MRONi}}}{dt} = \frac{Ad_{QROC_i}}{CN_{QROM_i}} - \frac{De_{MROC_i}}{CN_{MROM_i}} \quad \text{Eq. S66}$$

$$\frac{d_{\mathrm{MROPi}}}{dt} = \frac{Ad_{QROC_i}}{CP_{QROM_i}} - \frac{De_{MROC_i}}{CP_{MROM_i}} \quad \text{Eq. S67}$$

50. The dynamics of C ($\frac{d_{\mathrm{MLOCi}}}{dt}$), N ($\frac{d_{\mathrm{MLONi}}}{dt}$), and P ($\frac{d_{\mathrm{MLOPi}}}{dt}$) in *MLOM*$_i$

$$\frac{d_{\mathrm{MLOCi}}}{dt} = Ad_{QLOC_i} - De_{MLOC_i} \quad \text{Eq. S68}$$

$$\frac{d_{\mathrm{MLONi}}}{dt} = \frac{Ad_{QLOC_i}}{CN_{QLOM_i}} - \frac{De_{MLOC_i}}{CN_{MLOM_i}} \quad \text{Eq. S69}$$

$$\frac{d_{\mathrm{MLOPi}}}{dt} = \frac{Ad_{QLOC_i}}{CP_{QLOM_i}} - \frac{De_{MLOC_i}}{CP_{MLOM_i}} \quad \text{Eq. S70}$$

51. The dynamics of C ($\frac{d_{\mathrm{MOOCi}}}{dt}$), N ($\frac{d_{\mathrm{MOONi}}}{dt}$), and P ($\frac{d_{\mathrm{MOOPi}}}{dt}$) in *MOOM*$_i$

$$\frac{d_{\mathrm{MOOCi}}}{dt} = Ad_{QOOC_i} - De_{MOOC_i} \quad \text{Eq. S71}$$

$$\frac{d_{\mathrm{MOONi}}}{dt} = \frac{Ad_{QOOC_i}}{CN_{QOOM_i}} - \frac{De_{MOOC_i}}{CN_{MOOM_i}} \quad \text{Eq. S72}$$

$$\frac{d_{\mathrm{MOOPi}}}{dt} = \frac{Ad_{QOOC_i}}{CP_{QOOM_i}} - \frac{De_{MOOC_i}}{CP_{MOOM_i}} \quad \text{Eq. S73}$$

52. The dynamics of C ($\frac{d_{\mathrm{MMOC}}}{dt}$), N ($\frac{d_{\mathrm{MMON}}}{dt}$), and P ($\frac{d_{\mathrm{MMOP}}}{dt}$) in *MMOM*

$$\frac{d_{\mathrm{MMOC}}}{dt} = Ad_{QMOC} - De_{MMOC} \quad \text{Eq. S74}$$

$\frac{d_{\mathrm{MMON}}}{dt} = \frac{Ad_{QMOC}}{CN_{QMOM}} - \frac{De_{MMOC}}{CN_{MMOM}}$ Eq. S75

$\frac{d_{\mathrm{MMOP}}}{dt} = \frac{Ad_{QMOC}}{CP_{QMOM}} - \frac{De_{MMOC}}{CP_{MMOM}}$ Eq. S76

53. The dynamics of C ($\frac{d_{C_{MBA}}}{dt}$), N ($\frac{d_{N_{MBA}}}{dt}$), and P ($\frac{d_{P_{MBA}}}{dt}$) in *MBA*

$\frac{d_{C_{MBA}}}{dt} = A_{DOC} + C_{D2A} - C_{A2D} - Rg_a - Rm_a - S_{C_E} - D_{C_E}$ Eq. S77

$\frac{d_{N_{MBA}}}{dt} = \frac{A_{DOC}}{CN_{DOM}} + \frac{C_{D2A}}{CN_{MBD}} - \frac{C_{A2D}}{CN_{MBA}} - \frac{S_{C_E}}{CN_E} - \frac{D_{C_E}}{CN_{MBA}} + N_{As} - N_{mn}$ Eq. S78

$\frac{d_{P_{MBA}}}{dt} = \frac{A_{DOC}}{CP_{DOM}} + \frac{C_{D2A}}{CP_{MBD}} - \frac{C_{A2D}}{CP_{MBA}} - \frac{S_{C_E}}{CP_E} - \frac{D_{C_E}}{CP_{MBA}} + P_{im} - P_{mn}$ Eq. S79

54. The dynamics of C ($\frac{d_{C_{MBD}}}{dt}$), N ($\frac{d_{N_{MBD}}}{dt}$), and P ($\frac{d_{P_{MBD}}}{dt}$) in *MBD*

$\frac{d_{C_{MBD}}}{dt} = C_{A2D} - C_{D2A} - Rm_d$ Eq. S80

$\frac{d_{N_{MBD}}}{dt} = \frac{C_{A2D}}{CN_{MBA}} - \frac{C_{D2A}}{CN_{MBD}}$ Eq. S81

$\frac{d_{P_{MBD}}}{dt} = \frac{C_{A2D}}{CP_{MBA}} - \frac{C_{D2A}}{CP_{MBD}}$ Eq. S82

55. The dynamic of C ($\frac{dC_{\mathrm{E}}}{dt}$), N ($\frac{dN_{\mathrm{E}}}{dt}$), P ($\frac{dP_{\mathrm{E}}}{dt}$) in EFCs pool

$\frac{dC_{\mathrm{E}}}{dt} = S_{C_E} - D_{C_E}$ Eq. S83

$\frac{dN_{\mathrm{E}}}{dt} = \frac{S_{C_E}}{CN_E} - \frac{D_{C_E}}{CN_E}$ Eq. S84

$\frac{dP_{\mathrm{E}}}{dt} = \frac{S_{C_E}}{CP_E} - \frac{D_{C_E}}{CP_E}$ Eq. S85

56. Dynamics of DIP ($\frac{dDIP}{dt}$)

$\frac{dDIP}{dt} = \frac{((\boldsymbol{Ks_{DIP}}+DIP)^2}{((\boldsymbol{Ks_{DIP}}+DIP)^2+\boldsymbol{Qmax_{DIP}}\times Ks_{DIP})} \times (P_{wea} + D_{AROP_7} + DOP_{mn} + P_{mn} - P_{QIP_{ads}} - P_{plant} - P_{im})$

P_{plant} is estimated P uptake by plant Eq. S86

57. Dynamics of QIP ($\frac{dQIP}{dt}$)

$\frac{dQIP}{dt} = \frac{Qmax_{DIP}\times \boldsymbol{Ks_{DIP}}}{((\boldsymbol{Ks_{DIP}}+DIP)^2+\boldsymbol{Qmax_{DIP}}\times Ks_{DIP})} \times (P_{wea} + D_{AROP_7} + DOP_{mn} + P_{mn} - P_{QIP_{ads}} - P_{plant} - P_{im})$ Eq. S87

58. Dynamics of SIP ($\frac{dSIP}{dt}$)

$\frac{dSIP}{dt} = P_{QIP_{ads}} - P_{sec} - P_{ocl}$ Eq. S88

59. Dynamics of OIP ($\frac{dOIP}{dt}$)

$\frac{dOIP}{dt} = P_{ocl}$ Eq. S89

60. Dynamics of PIP ($\frac{dPIP}{dt}$)

$\frac{dPIP}{dt} = P_{pri}$ Eq. S90

61. Dynamics of IN_1 ($\frac{dN_1}{dt}$)

$\frac{dN_1}{dt} = N_{mn} + N_{fix} - N_{assim} - N_{nitri} - N_{plant}$ Eq. S91

62. Dynamics of IN_2 ($\frac{dN_2}{dt}$)

$\frac{dN_2}{dt} = N_{nitri} - N_{denitri}$ Eq. S92

Note: Bold terms in the equations above are input parameters, which are described and given in table S5-S8. CN_i and CP_i in Eqs. (S42-S85) denote the C/N and C/P ratio of the corresponding microbial, EFC or SOM pool i, respectively.

Supplementary Figures

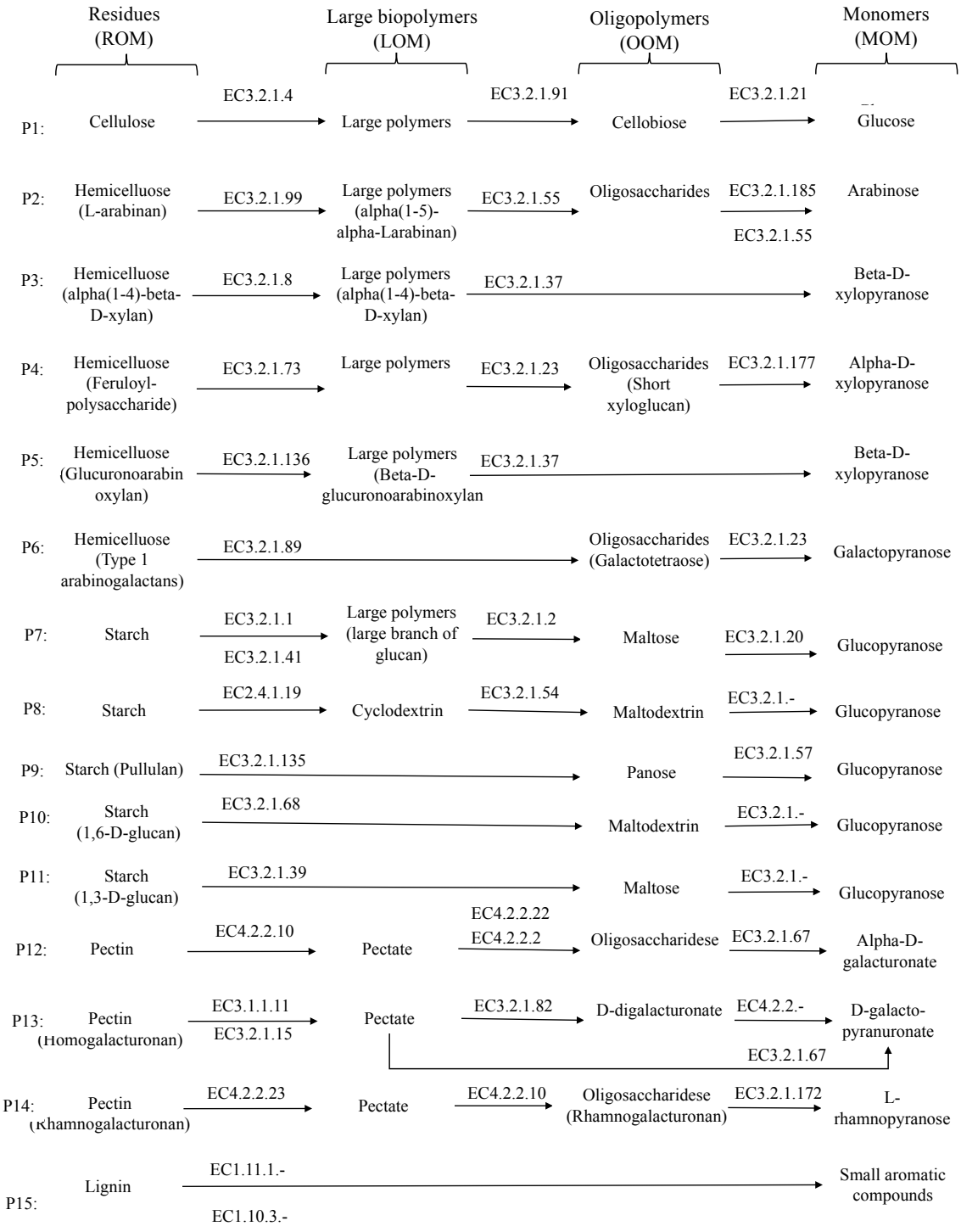

Fig. S1. Metagenomics-informed lignocellulose-containing soil organic matter (SOM) decomposition pathways and corresponding enzymes identified in the Panama soil samples, where EC refers to the Enzyme Classification number

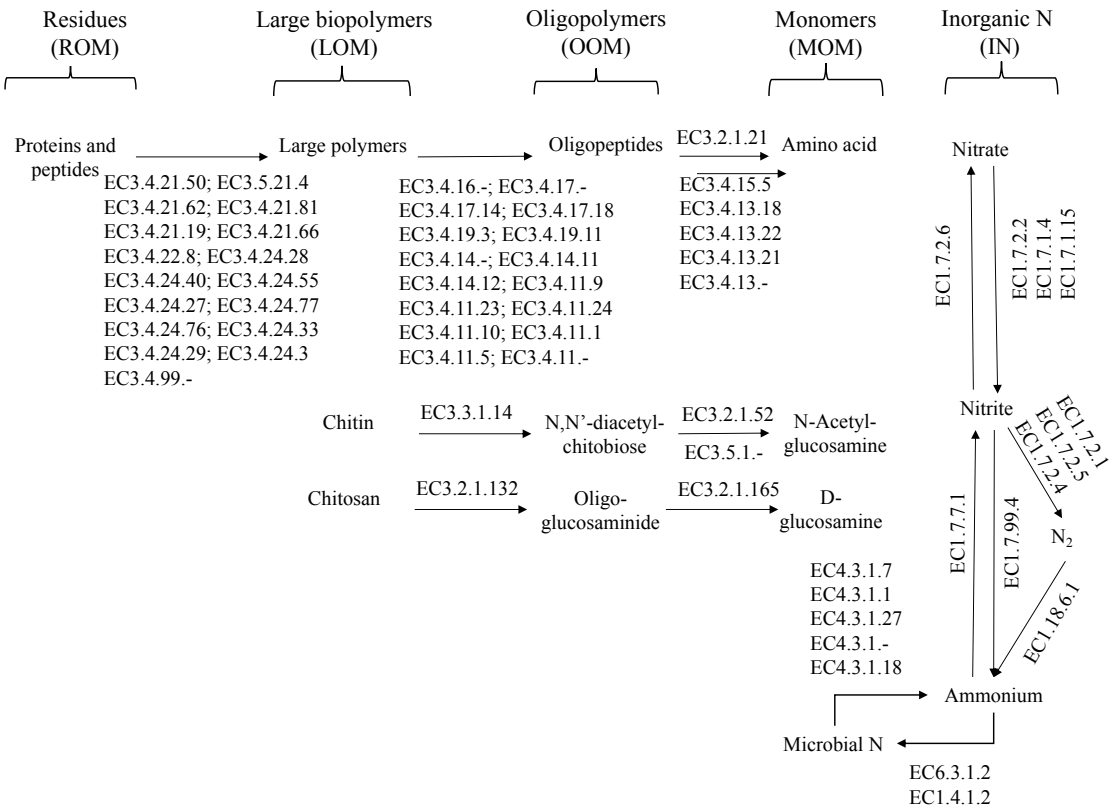

Fig. S2. Metagenomics-informed nitrogen (N)-containing SOM decomposition and mineralization pathways and corresponding enzymes identified in the Panama soil samples, where EC refers to the Enzyme Classification numbers.

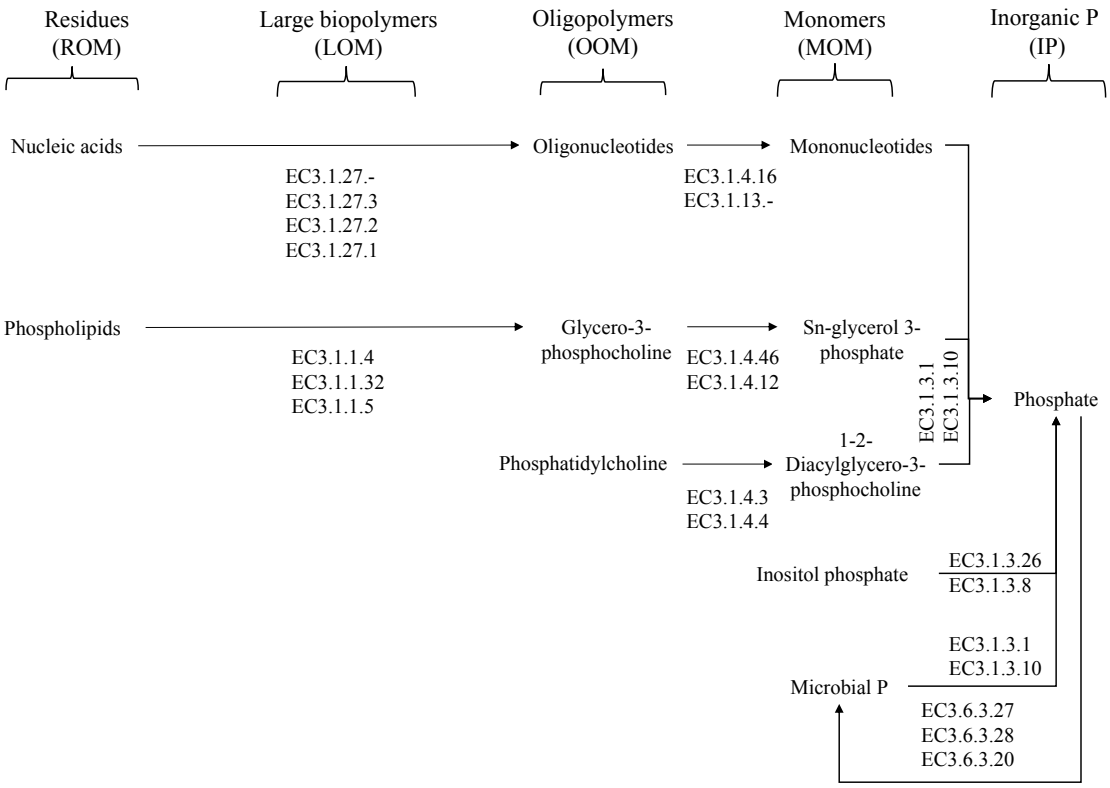

Fig S3. Metagenomics-informed P-containing SOM decomposition and mineralization pathways and corresponding enzymes identified in the Panama soil samples, where EC refers to the Enzyme Classification numbers.

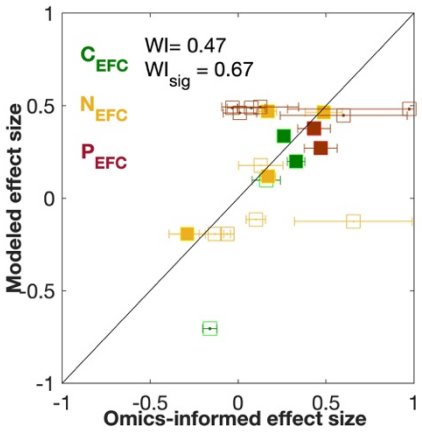

Fig. S4. Modeled and metagenomics-informed effect sizes of enzyme function groups (EFCs) between the control and P-fertilized soils. Here the effect size is defined as the $\log_2$ fold change of gene abundance of the EFC in the control plots relative to that in the P-fertilized soils. The error bar represents the standard deviation of metagenomics-informed effect size of each EFC. The filled symbols indicate that the difference of the EFC between the control soils and the P-fertilized soils is statistically significant (q-value <0.05). The Willmott index of agreement (WI) for all EFCs is 0.47 (P value <0.05), while the index (WI_{sig}) for EFCs with statistically significant effect size is 0.67 (P value <0.05). C_{EFC}, N_{EFC}, P_{EFC} are EFCs for decomposing lignocellulose-containing, N-containing, and P-containing SOM, respectively.

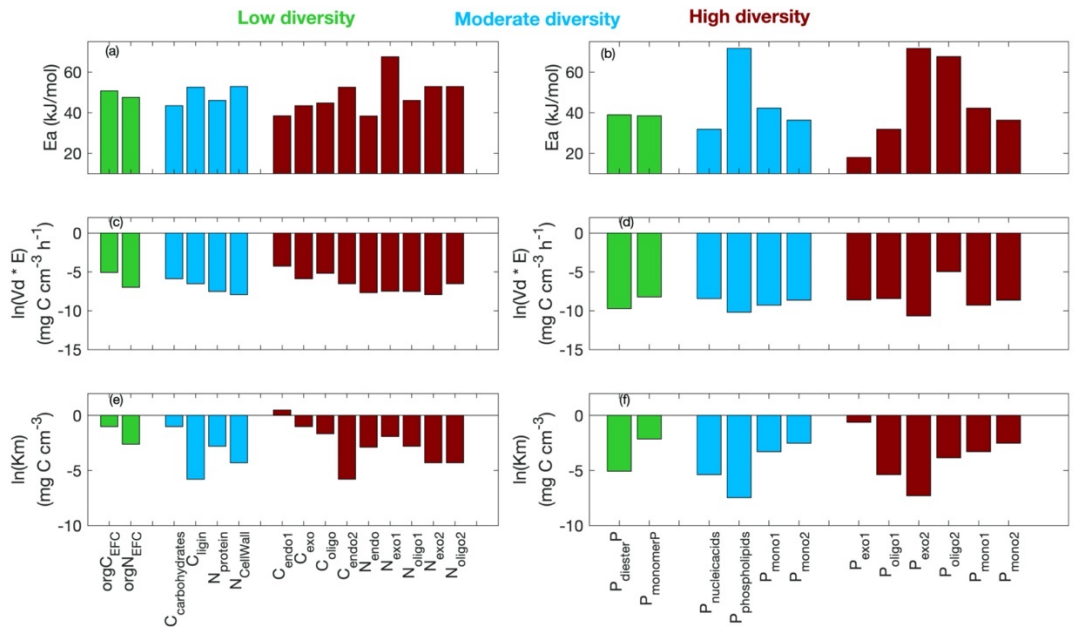

Fig. S5. Effects of enzyme functional diversity of soil microbial communities on decomposition kinetics of enzyme functional classes (EFCs): (a-b) Activation energy (kJ/mol); (c-d) Potential EFC activity (Vd *E); and (e-f) Substrate affinity (K_m). Three version of models were compared: $CoMEND_H$ included all metagenomics-informed 22 EFCs for SOM decomposition and thus represented high enzyme functional diversity. $CoMEND_M$ only included 15 EFCs for SOM decomposition and thus represented moderate functional diversity of microbial community. $CoMEND_L$ included 11 clusters of EFCs and represented low functional diversity of microbial community.

476 **Supplementary Tables**

477 **Table S1.** Classification of soil enzyme functional groups (EFCs) in Panamanian soils.

Biogeochemical processes	EFC classification rule 1		EFC classification rule 2		Numbers of enzymes	EFC function
	EFC 1	The chemical component of substrate that the EFC acts on	EFC 2	The location of EFC cleaved chemical component/the function of the EFC		
Lignocellulose-containing soil organic matter (SOM) decomposition	$C_{carbohydrates}$	Carbohydrates	C_{endo1}	Internal C-O bonds	16	Decomposition of carbohydrate residue
		Carbohydrates	C_{exo1}	Terminal C-O bonds	9	Decomposition of large polymers of carbohydrate
		Carbohydrates	C_{oigo1}	C-O bonds	11	Decomposition of oilgosaccharides
	C_{lignin}	Lignin	C_{endo2}	Internal C-C or C-O bonds	3	Decomposition of lignin
N-containing SOM decomposition and mineralization	$N_{proteins}$	Proteins	N_{endo1}	Internal C-N bonds	17	Decomposition of protein or peptides chains
		Proteins	N_{exo1}	Terminal C-N bonds	16	Decomposition of polypeptides
		Proteins	N_{oligo1}	C-N bonds	5	Decomposition of oligopeptides
	$N_{cellwall}$	Cell wall N component	N_{exo2}	Terminal C-O bonds	2	Decomposition of cell wall N residues
		Cell wall N component	N_{oligo2}	C-O bonds	2	Decomposition of oligosaccharides
	$N_{microbialN}$	Microbial assimilated N	N_{mono}	C-N bond	5	Microbial intracellular N mineralization
	$N_{inorganicN}$	Inorganic N	N_{inN1}	Nitrification	2	Nitrification
		Inorganic N	N_{inN2}	Denitrification	3	Denitrification
		Inorganic N	N_{inN3}	N assimilation	6	N assimilation
		Inorganic N	N_{inN4}	N fixation	1	N fixation
P-containing SOM decomposition and mineralization	$P_{nucleicacids}$	Nucleic acids	P_{exo1}	Terminal phosphoester bonds	4	Decomposition of nucleic acids residues
		Nucleic acids	P_{oligo1}	Phosphoester bonds	2	Decomposition of oligonucleotides
	$P_{phospholipids}$	Phospholipids	P_{exo2}	C-O bond	3	Decomposition of phospholipids
		Phospholipids	P_{oligo2}	Phosphoester bond	3	Decomposition of lyso-phosphatidylcholine
	$P_{monomerP}$	Inositol P	P_{mono1}	Phosphoester bond	2	Inositol P biochemical mineralization
		Monomer P	P_{mono2}	Phosphoester bond	2	General monophosphate biochemical mineralization
	$P_{microbialP}$	Microbial assimilated P	P_{mono3}	Phosphoester bond	2	Biological P mineralization
	P_{mono3}	Inorganic P	P_{inP}	P immobilization	3	P immobilization

Table S2. The modification of environmental factors on reaction rate parameters in the CoMEND model

The reaction rate parameters modified by environmental factors	Modification function	Eq. ID
Kinetic parameters (Vd_j and Ks_j) for SOM decomposition in Eqs. (S1-S3) and Eqs. (S24-S31),	$Vd_j = \boldsymbol{Vd_j} \times f(\psi) \times f(T) \times f(pH)$, where j denotes corresponding EFC in the equation.	Eq. S93
	$Ks_j = \boldsymbol{Ks_j} \times f(T)$, where j denotes corresponding EFC in the equation.	Eq. S94
	Soil water potential (ψ) modification factor $f(\psi) = \begin{cases} 0.0 & \psi < \psi_{min} \\ 1.0 - [\frac{\ln(\frac{\psi}{\boldsymbol{\psi_{FC}}})}{\ln(\frac{\boldsymbol{\psi_{min}}}{\boldsymbol{\psi_{FC}}})}]^{1.2} & \psi_{min} < \psi \le \psi_{FC}, \\ 1.0 & \psi > \psi_{FC} \end{cases}$	Eq. S95
	Soil temperature (T) modificatory factor $f(T) = e^{[-\frac{\boldsymbol{Ea_j}}{R}(\frac{1}{T}-\frac{1}{T_{ref}})]}$, $T_{ref} = 20°C$	Eq. S96
	Soil pH modification factor $f(pH) = \mathrm{e}^{[-(\frac{pH-\boldsymbol{pH_{opt_j}}}{pH_{sen_j}})^2]}$	Eq. S97
SOM adsorption/desorption rate in Eqs. (S4-S19)	$k_{ads_j} = \boldsymbol{k_{ads_j}} \times f(T)$, where j denotes corresponding SOM in the equation	Eq. S98
	$k_{des_j} = \boldsymbol{k_{des_j}} \times f(T)$, where j denotes corresponding SOM in the equation	Eq. S99
Inorganic P adsorption/desorption rate in Eqs. (S22-S23)	$\gamma_{QIP_{ads}} = \boldsymbol{\gamma_{QIP_{ads}}} \times f(T)$	Eq. S100
	$\gamma_{des} = \boldsymbol{\gamma_{des}} \times f(T)$	Eq. S101
Microbial growth rate parameters in Eqs. (S32-S35)	$Vg = \boldsymbol{Vg} \times f(T)$	Eq. S102
	$Vm = \boldsymbol{Vm} \times f(T)$	Eq. S103
	$Ks_{DOC} = \boldsymbol{Ks_{DOC}} \times f(T)$	Eq. S104
	$Yg = \boldsymbol{Yg_0} - \boldsymbol{k_{Yg}}(T - T_{ref})$	Eq. S105
Microbial mortality rate parameter in Eq. (S36)	$\gamma_M = \boldsymbol{\gamma_M} \times L_c$	Eq. S106
	$L_c = \frac{\lvert\psi\rvert^{\boldsymbol{b}}}{\lvert\psi\rvert^{\boldsymbol{b}} + \lvert\boldsymbol{\psi_D}\rvert^{\boldsymbol{b}}}$	Eq. S107
Microbial dormancy rate parameter in Eq. (S37)	$Vm_{A2D} = \boldsymbol{Vm} \times f(T) \times f_{A2D}(\psi)$	Eq. S108
	$f_{A2D}(\psi) = \frac{\lvert\psi\rvert^{\boldsymbol{c}}}{\lvert\psi\rvert^{\boldsymbol{c}} + \lvert\boldsymbol{\psi_{A2D}}\rvert^{\boldsymbol{c}}}$	Eq. S109
Microbial resuscitation rate parameter in Eq. (S38)	$Vm_{D2A} = Vm_0 \times f(T) \times f_{D2A}(\psi)$	Eq. S110
	$f_{D2A}(\psi) = \frac{\lvert\psi\rvert^{\boldsymbol{c}}}{\lvert\psi\rvert^{\boldsymbol{c}} + \lvert\boldsymbol{\psi_{D2A}}\rvert^{\boldsymbol{c}}}$	Eq. S111

Note: Bold terms in the equations are input parameters, which are described and given in Supplementary information (SI) Data S4.

Supplementary equations: Components fluxes and dynamics of SOM pools in the CoMEND model.

Table S3. Chemical components, representative molecular formula and C/N and C/P ratio of SOM pool.

SOM	Chemical component	Representative molecular formula	C/N	C/P	Source
$AROM_1$, $ALOM_1$,$AOOM_1$, $MROM_1$,$MLOM_1$,$MOOM_1$	Carbohydrates related	$(C_6H_{10}O_5)_n$	-	-	[26]
$AROM_2$, $MROM_2$	Lignin related	$(C_{10}H_{12}O_3)_n$	-	-	[26]
$AROM_3$, $ALOM_3$, $AOOM_3$, $MROM_3$,$MLOM_3$, $MOOM_3$	Proteinaceous	$(C_{20}H_{30}O_5N_5)_n$	3.5	-	[26]
$AROM_4$, $AOOM_4$, $MROM_4$,$MOOM_4$	Cell wall-N component	$(C_8H_{13}NO_5)_n$	6.9	-	Brenda database[14]
$AROM_5$, $AOOM_5$, $MROM_5$,$MOOM_5$	Nucleic acids related	$(C_{10}H_{14}N_4O_8P)_n$	2.1	3.9	[26]
$AROM_6$, $AOOM_6$, $MROM_6$,$MOOM_6$	Phospholipids related	$C_{33}H_{58}O_{24}P_6$	-	12.8	Brenda database[14]
$AROM_7$	Inositol P	$(C_6H_{18}O_{24}P_6)_n$	-	1.4	Brenda database[14]

Supplementary Notes: References cited in the SI

1 Kay, J. E. *et al.* The Community Earth System Model (CESM) Large Ensemble Project: A Community Resource for Studying Climate Change in the Presence of Internal Climate Variability. *Bulletin of the American Meteorological Society* **96**, 1333-1349, doi:10.1175/bams-d-13-00255.1 (2015).

2 Yao, Q. M. *et al.* Community proteogenomics reveals the systemic impact of phosphorus availability on microbial functions in tropical soil. *Nat Ecol Evol* **2**, 499-509, doi:10.1038/s41559-017-0463-5 (2018).

3 Tfaily, M. M. *et al.* Sequential extraction protocol for organic matter from soils and sediments using high resolution mass spectrometry. *Anal Chim Acta* **972**, 54-61, doi:10.1016/j.aca.2017.03.031 (2017).

4 Tfaily, M. M. *et al.* Advanced Solvent Based Methods for Molecular Characterization of Soil Organic Matter by High-Resolution Mass Spectrometry. *Anal Chem* **87**, 5206-5215, doi:10.1021/acs.analchem.5b00116 (2015).

5 Darch, T. *et al.* Assessment of bioavailable organic phosphorus in tropical forest soils by organic acid extraction and phosphatase hydrolysis. *Geoderma* **284**, 93-102, doi:10.1016/j.geoderma.2016.08.018 (2016).

6 Mirabello, M. J. *et al.* Soil phosphorus responses to chronic nutrient fertilisation and seasonal drought in a humid lowland forest, Panama. *Soil Research* **51**, 215-221, doi:https://doi.org/10.1071/SR12188 (2013).

7 Schwendenmann, L. & Pendall, E. Effects of forest conversion into grassland on soil aggregate structure and carbon storage in Panama: evidence from soil carbon fractionation and stable isotopes. *Plant Soil* **288**, 217-232, doi:10.1007/s11104-006-9109-0 (2006).

8 Yang, X., Thornton, P. E., Ricciuto, D. M. & Post, W. M. The role of phosphorus dynamics in tropical forests - a modeling study using CLM-CNP. *Biogeosciences* **11**, 1667-1681, doi:10.5194/bg-11-1667-2014 (2014).

9 Yang, X. J., Thornton, P. E., Ricciuto, D. M. & Hoffman, F. M. Phosphorus feedbacks constraining tropical ecosystem responses to changes in atmospheric CO2 and climate. *Geophys Res Lett* **43**, 7205-7214, doi:10.1002/2016gl069241 (2016).

10 Manzoni, S., Schaeffer, S. M., Katul, G., Porporato, A. & Schimel, J. P. A theoretical analysis of microbial eco-physiological and diffusion limitations to carbon cycling in drying soils. *Soil Biol Biochem* **73**, 69-83, doi:10.1016/j.soilbio.2014.02.008 (2014).

11 Jansson, J. K. & Hofmockel, K. S. The soil microbiome - from metagenomics to metaphenomics. *Curr Opin Microbiol* **43**, 162-168, doi:10.1016/j.mib.2018.01.013 (2018).

12 Bouskill, N. J. *et al.* Belowground Response to Drought in a Tropical Forest Soil. II. Change in Microbial Function Impacts Carbon Composition. *Frontiers in Microbiology* **7**, doi:ARTN 323 10.3389/fmicb.2016.00323 (2016).

13 Bouskill, N. J. *et al.* Belowground Response to Drought in a Tropical Forest Soil. I. Changes in Microbial Functional Potential and Metabolism. *Frontiers in Microbiology* **7**, doi:ARTN 525 10.3389/fmicb.2016.00525 (2016).

14 Scheer, M. *et al.* BRENDA, the enzyme information system in 2011. *Nucleic Acids Res* **39**, D670-D676, doi:10.1093/nar/gkq1089 (2011).
15 Duan, Q. Y., Sorooshian, S. & Gupta, V. Effective and Efficient Global Optimization for Conceptual Rainfall-Runoff Models. *Water Resour Res* **28**, 1015-1031, doi:Doi 10.1029/91wr02985 (1992).
16 Wang, G. S., Xia, J. & Chen, J. Quantification of effects of climate variations and human activities on runoff by a monthly water balance model: A case study of the Chaobai River basin in northern China. *Water Resour Res* **45**, doi:Artn W00a11 10.1029/2007wr006768 (2009).
17 Turner, B. L. & Wright, S. J. The response of microbial biomass and hydrolytic enzymes to a decade of nitrogen, phosphorus, and potassium addition in a lowland tropical rain forest. *Biogeochemistry* **117**, 115-130, doi:10.1007/s10533-013-9848-y (2014).
18 Yang, X., Post, W. M., Thornton, P. E. & Jain, A. The distribution of soil phosphorus for global biogeochemical modeling. *Biogeosciences* **10**, 2525-2537, doi:10.5194/bg-10-2525-2013 (2013).
19 Kogel-Knabner, I. in *Nucleic acids and proteins in soil* (eds Paolo Nannipieri & Kornelia Smalla) 23-48 (Springer, 2006).
20 Bugg, T. D. H., Ahmad, M., Hardiman, E. M. & Rahmanpour, R. Pathways for degradation of lignin in bacteria and fungi. *Nat Prod Rep* **28**, 1883-1896, doi:10.1039/c1np00042j (2011).
21 Paton, S. 2017 meteorological and hydrological summary for Barro Colorado island. (Simithsonian Tropical Research Institute, 2017).
22 Kaspari, M. *et al.* Multiple nutrients limit litterfall and decomposition in a tropical forest. *Ecol Lett* **11**, 35-43, doi:10.1111/j.1461-0248.2007.01124.x (2008).
23 Wright, S. J. *et al.* Potassium, phosphorus, or nitrogen limit root allocation, tree growth, or litter production in a lowland tropical forest. *Ecology* **92**, 1616-1625 (2011).
24 Ostertag, R., Marin-Spiotta, E., Silver, W. L. & Schulten, J. Litterfall and decomposition in relation to soil carbon pools along a secondary forest chronosequence in Puerto Rico. *Ecosystems* **11**, 701-714, doi:10.1007/s10021-008-9152-1 (2008).
25 Winkler, U. & Zotz, G. Highly efficient uptake of phosphorus in epiphytic bromeliads. *Ann Bot-London* **103**, 477-484, doi:10.1093/aob/mcn231 (2009).
26 Riley, W. J. *et al.* Long residence times of rapidly decomposable soil organic matter: application of a multi-phase, multi-component, and vertically resolved model (BAMS1) to soil carbon dynamics. *Geosci Model Dev* **7**, 1335-1355, doi:10.5194/gmd-7-1335-2014 (2014).
27 Torabizadeh, H. All proteins have a basic molecular formula. *World Academy of Science, Engineering and Technology* **5**, 961-965 (2011).
28 Wang, G. S., Post, W. M. & Mayes, M. A. Development of microbial-enzyme-mediated decomposition model parameters through steady-state and dynamic analyses. *Ecol Appl* **23**, 255-272, doi:Doi 10.1890/12-0681.1 (2013)
29 Xu, X. F., Thornton, P. E. & Post, W. M. A global analysis of soil microbial biomass carbon, nitrogen and phosphorus in terrestrial ecosystems. *Global Ecol Biogeogr* **22**, 737-749, doi:10.1111/geb.12029 (2013).

30 Sayer, E. J. *et al.* Variable Responses of Lowland Tropical Forest Nutrient Status to Fertilization and Litter Manipulation. *Ecosystems* **15**, 387-400, doi:10.1007/s10021-011-9516-9 (2012).
31 Heineman, K. D., Turner, B. L. & Dalling, J. W. Variation in wood nutrients along a tropical soil fertility gradient. *New Phytol* **211**, 440-454, doi:10.1111/nph.13904 (2016).